

## Synthesis, Characterization and Properties of CeO<sub>2</sub>-doped TiO<sub>2</sub> Composite Nanocrystals

Oman ZUAS\*, Nuryatini HAMIM

Process Technology and Catalysis Division, Research Centre for Chemistry (RCC), Indonesian Institute of Sciences (LIPI), Kawasan PUSPIPTEK Serpong, 15314, Tangerang, Banten, Indonesia

**crossref** <http://dx.doi.org/10.5755/j01.ms.19.4.2732>

Received 29 October 2012; accepted 10 March 2013

Pure TiO<sub>2</sub> and CeO<sub>2</sub>-doped TiO<sub>2</sub> (3 % CeO<sub>2</sub>-97 %TiO<sub>2</sub>) composite nanocrystals were synthesized via co-precipitation method and characterized using TGA, XRD, FTIR, DR-UV-vis and TEM. The XRD data revealed that the phase structure of the synthesized samples was mainly in pure anatase having crystallite size in the range of 7 nm–11 nm. Spherical shapes with moderate aggregation of the crystal particles were observed under the TEM observation. The presence of the CeO<sub>2</sub> at TiO<sub>2</sub> site has not only affected morphologically but also induced the electronic property of the TiO<sub>2</sub> by lowering the band gap energy from 3.29 eV ( $E_g$ -Ti) to 3.15 eV ( $E_g$ -CeTi). Performance evaluation of the synthesized samples showed that both samples have a strong adsorption capacity toward Congo red (CR) dye in aqueous solution at room temperature experiment, where the capacity of the CeTi was higher than the Ti sample. Based on DR-UV data, the synthesized samples obtained in this study may also become promising catalysts for photo-assisted removal of synthetic dye in aqueous solution.

**Keywords:** TiO<sub>2</sub>, CeO<sub>2</sub>, metal oxide, nanocrystal, synthetic dye.

### 1. INTRODUCTION

Development of semiconductor nanomaterials having tailorable function has attracted much attention in the area for solving energy and environmental issues. Among the important transition metal semiconductors, titanium dioxide (TiO<sub>2</sub>) is probably one of the most widely studied in heterogeneous catalysis, in solar cell, in coating technology and in electrical devices [1], due to its tremendous properties including inexpensive material, high chemical stability, high mechanical strength, photo activated material, and environmentally friendly [2–4].

There has been a concrete effort to enhance the functionality properties of TiO<sub>2</sub> by composing with other transition metal semiconductors such as Al<sub>2</sub>O<sub>3</sub> [5], CeO<sub>2</sub> [6], CuO [7], Fe<sub>2</sub>O<sub>3</sub> [8], SnO<sub>2</sub> [9], SiO<sub>2</sub> [5, 10], WO<sub>3</sub> [11], ZnO [12] and ZrO<sub>2</sub> [5, 10]. The beneficial effects of such metal oxide semiconductors in relation with their existence at TiO<sub>2</sub> site is evidenced by increasing in the surface area, by decreasing in particle size, and positive change in optical and electrical properties [5, 9, 13–16]. In term of nano dimensional particle and high surface area of pure TiO<sub>2</sub> and metal oxide-TiO<sub>2</sub> nanocomposites, these materials have the possibility of being applied as an adsorbent for removal of pollutants. Generally speaking, adsorbents with nano-scale in particle diameter would have high surface area and determine their adsorption capacity [17–19], which further allows for more adsorbate to attach on the the surface of the adsorbent [20, 21].

To overcome the drawback regarding the limitations of the TiO<sub>2</sub> particle with micro-scale in diameter, such as limited surface-to-volume ratio which determines their adsorption capacity for low concentration of target

pollutant, nanostructured TiO<sub>2</sub>-based materials offer advantages and have been previously reported as materials with better properties like adsorption capacity and selectivity [17, 20].

In this study, pure TiO<sub>2</sub> and CeO<sub>2</sub>-doped TiO<sub>2</sub> were synthesized by co-precipitation method. The structural and morphology of the synthesized samples were characterized using TGA, XRD, DR-UV-vis, FTIR and TEM, while the activity was evaluated for their adsorption performance for CR dye in aqueous solution.

### 2. EXPERIMENTAL DETAILS

#### 2.1. Materials

All chemicals were analytic grade and used as received without further purification. Titanium tetrachloride (TiCl<sub>4</sub>, > 99 %, Merck-Germany), cerium (III) nitrate hexahydrate (Ce(NO<sub>3</sub>)<sub>3</sub>·6H<sub>2</sub>O, 99.9 %, Merck-Germany), aqueous ammonia solution (NH<sub>3</sub>·H<sub>2</sub>O, 25 %, Merck-Germany), sodium hydroxide (NaOH, 99.8 %, Merck-Germany), N-Cetyl-N,N,N-trimethylammonium bromide (CTAB, 98 %, Merck-Germany), Congo red dye (C.I. 22120, CAS No. 573-58-0, 97 %, Sigma-Aldrich, Germany). Purified water was produced using Millipore purified water system.

#### 2.2. Methods

**Synthesis of pure TiO<sub>2</sub> and CeO<sub>2</sub>-doped TiO<sub>2</sub>.** Pure TiO<sub>2</sub> (denoted as Ti) and composite of ceria-doped titania (3 wt% of CeO<sub>2</sub> – 97 wt% of TiO<sub>2</sub>, denoted as CeTi) were synthesized following the method in our previous work with modification [22]. Typically, an appropriate amount of Ce(NO<sub>3</sub>)<sub>3</sub>·6H<sub>2</sub>O, to give 3 %wt of CeO<sub>2</sub> in the final product, was added into CTAB:TiCl<sub>4</sub> mixture solutions (0.2 molar ratio). The mixture was then precipitated using an aqueous ammonia solution (NH<sub>3</sub>·H<sub>2</sub>O, 25 %) under

\*Corresponding author. Tel.: +62-21-7560929; fax.: +62-21-7560549.  
E-mail address: [oman.zuas@lipi.go.id](mailto:oman.zuas@lipi.go.id) (O Zuas)

vigorous stirring until the pH 10 of the solution was reached. The colloidal solution was aged at 55 °C–60 °C for 6 h under stirring. After that, the colloidal solution was centrifuged at 8000 rpm for 10 min to remove the supernatant. Wet solid material obtained was then washed thoroughly with distilled water for several times until no chloride ions could be detected in the filtrate (visual observations using silver nitrate as a test reagent). The wet solid material was dried at 100 °C for 12 h to produce dry solid materials. Dry solid materials were then calcined at 500 °C for 4 h in open air in a tube box muffle furnace to produce CeTi composite nanocrystals. The pure TiO<sub>2</sub> (denoted as pure Ti) was also synthesized with the same procedure without addition of Ce precursor according to notes above in this chapter.

**Sample characterization.** The X-ray diffraction (XRD) patterns were obtained at room temperature on a Philips-Type PW1710 X-ray diffractometer with Cu ( $k = 1.5406 \text{ \AA}$ ) irradiation and scanned  $2\theta$  in the range of 10°–80° at a scanning speed of 1.2°/min. The diffuse reflectance-UV visible (DR-UV-Vis) spectra were recorded on a Shimadzu UV2450 spectrophotometer under ambient temperature and BaSO<sub>4</sub> was used as a reference. Thermogravimetric analysis (TGA) was conducted on a TGA DuPont 951 in the presence of static air at a heating rate of 100 °C/min from 25 °C to 900 °C. Surface functional groups were examined using a FTIR-2000 Perkin Elmer from the scanning range of 4000 cm<sup>-1</sup>–500 cm<sup>-1</sup>. Surface morphology of the sample was observed from electron micrographs obtained with a Philips CM30 Transmission Electron Microscope (TEM) operated at 200 kV.

**Dye adsorption testing.** The activity performance of the synthesized samples was tested for their ability for removing textile dye in aqueous solution. Congo red (CR), a carcinogenic textile dye, was used as the model of organic pollutant. The adsorption experiment of CR dye was conducted in 15 ml capped glass tubes containing 5 ml of CR solution (15 mg/g) and 15 mg of synthesized composite nanocrystals. The sample-containing glass tubes were then placed in a Certomat WR-Braun Biotech International temperature-controlled water bath shaker with a constant agitation speed (120 rpm) and 25 °C ± 1 °C. After a certain period of time, the glass tubes were taken. The CR filtrate was separated from the solid material. Absorbance of the filtrate was then measured using a U-3501 Shimadzu UV-Vis-NIR spectrophotometer at wavelength maximum of the CR ( $\lambda_{\text{max}} = 500 \text{ nm}$ ). The concentration of the CR that remains in the sample solution was calculated from a calibration curve. The percentage of CR adsorption expressed as follows:

$$\% \text{ Adsorption} = ((C_0 - C_t)/C_0) \times 100 \% \quad (1)$$

where  $C_0$  is the initial concentration of CR dye, mg/l;  $C_t$  is the concentration of CR dye remaining at time  $t$ , mg/l.

### 3. RESULTS AND DISCUSSION

#### 3.1. Characterization

The TGA pattern of the dried solids of the composite nanocrystal precursors are given in Fig. 1. As shown in Fig. 1, the main mass loss occurs at temperature below 450 °C for both composite precursors, indicating the

existence of physical adsorption or chemically bonded hydroxyl groups. In general, the thermal decomposition of both precursors occurred in three main loss stages with the total mass loss of about 65.33 %. The first stage occurred in temperature ranging from 25 °C to 105 °C with mass loss of about 46.29 %. This stage was attributed to the evaporation of adsorbed water. The second stage is observed from TG curve at temperature range of 105 °C–450 °C which was attributed to decomposition of CTAB template and dehydroxylation of the surface, while both pure Ti and CeTi oxide were formed. The third stage occurred at temperature above 450 °C and little further mass loss in the TG curve is observed which may be due to removal of little residual CTAB template.

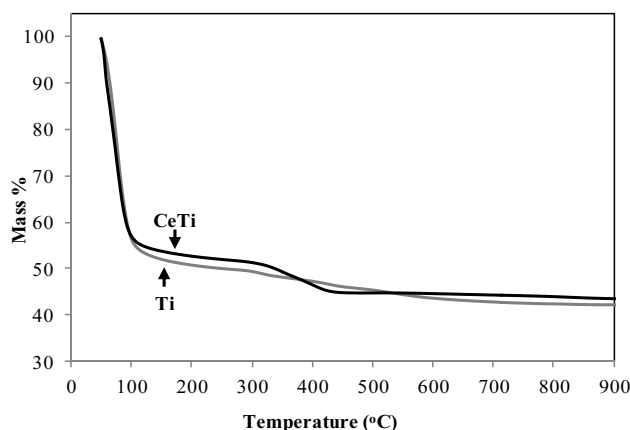


**Fig. 1.** TGA pattern of the dried solid materials of the composite nanocrystal precursors

The XRD diffraction patterns of the synthesized composite nanocrystals are shown in Fig. 2. The diffraction peaks ( $2\theta$ ) of the synthesized samples at about 25°, 38°, 48°, 54°, 55°, 63°, 69°, 70° and 76° can be ascribed to the reflection of (101), (004), (200), (105), (116), (211), (213), (204) and (116) planes of the TiO<sub>2</sub>, respectively, which are consistent with the standard JCPDS values of anatase TiO<sub>2</sub> (JCPDS Card No. 21-1272) [23-25]. The XRD patterns of both samples exhibit sharp and well defined peaks for anatase TiO<sub>2</sub>, indicating that the materials are present in a good crystallinity phase. No rutile peaks can be observed in the XRD spectra of both synthesized samples, indicating that the temperature used in the samples calcination suitable for the formation of anatase phase. In addition, no peaks of CeO<sub>2</sub> in the synthesized CeTi spectrum is observed, implying that the very low CeO<sub>2</sub> precursor added during synthesis process may be the reason, or the metal has been well-dispersed in the TiO<sub>2</sub> host lattices as a small cluster [24].

The average crystallite size of the synthesized samples were calculated from the full-width at half-maximum (FWHM) of anatase (101) reflection (Fig. 2) using Scherrer's formula [26],

$$D = k\lambda / \beta \cos\theta, \quad (2)$$

where  $D$  is the crystallite size,  $k$  is a constant ( $= 0.9$  assuming that the particles are spherical),  $\lambda$  is the wavelength of the X-rays,  $\beta$  is the FWHM, and  $\theta$  is the diffraction angle, in radians. The average crystallite size of pure Ti and CeTi samples was found to be 11 nm and

7 nm, respectively. Difference between crystallite size of pure Ti and CeTi samples is 4 nm. Decreasing in the crystallite size might be ascribed as result of a broadening effect due to incorporation of CeO<sub>2</sub> into TiO<sub>2</sub> matrix. In a word, lowering the intensity and broadening the width of the anatase (101) reflection led to decrease the calculated crystallite size correspondingly. From insert of Fig. 2, it can also be observed that un-shifted the peak (101) reflection of anatase crystal of the CeTi compared with pure Ti sample (in insert of Fig. 2) indicates that CeO<sub>2</sub> did not perturb the TiO<sub>2</sub> lattices. The CeO<sub>2</sub> concentration is rather low, therefore, it is possible that TiO<sub>2</sub> lattice distortions, resulting in XRD peak shift, are not visible in the powder XRD patterns.

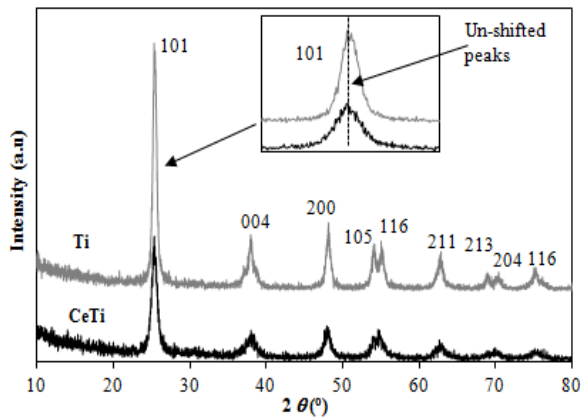


Fig. 2. XRD pattern of the synthesized composite nanocrystal

Fig. 3 represents the FTIR spectra of the synthesized composites. As it can be seen in Fig. 3, the IR band at 3000–3200 cm<sup>-1</sup> corresponds to the stretching vibration of O–H bond from hydroxyl [27]. The IR peak at about 1630 cm<sup>-1</sup> is assigned to the O–H bending of molecularly physisorbed water [28]. A characteristic band with strong and wide absorption at lower energy region (<800 cm<sup>-1</sup>) is attributed to the formation of anatase O–Ti–O lattice [28]. The peak around 650 cm<sup>-1</sup> can be ascribed to the stretching vibration mode of metal oxide (M–O) [29]. This stretching vibration mode of the metal oxide supports the XRD data, where the metal oxides Ti and CeTi were formed.

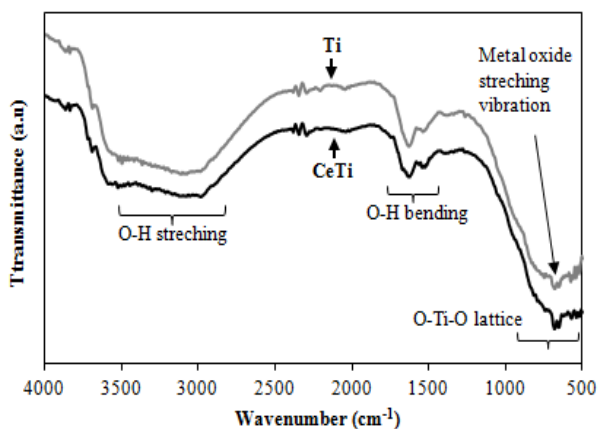


Fig. 3. FTIR spectra of the synthesized composite nanocrystals

The light absorbance characteristics of the synthesized samples in the UV-visible range were investigated from the diffuse reflectance spectra [30–32]. The measured

reflectance spectra obtained were transformed into Kubelka-Munk function ( $F(R)$ ),

$$F(R) = (1 - R)^2 / 2R, \quad (3)$$

where  $R$  is the reflectance value of the sample. Moreover, the absorption edge values of the samples were determined by plotting between the K-M function and wavelength as shown in Fig. 4. After that, the estimated band gap energy ( $E_g$ ) of the samples was generated by substituting the obtained absorption edge ( $\lambda$ ) values into the formula below [30]:

$$E_g \text{ (eV)} = 1236 / \lambda \text{ (nm)}. \quad (4)$$

As it can be seen from Fig. 4, the absorption edges of CeTi (392 nm) shifted to higher wavelength (red shift) compared to the absorption edges of Ti (374 nm) as related to change of band gap ( $E_g$ ) due to the presence of Ce in TiO<sub>2</sub> host lattices. The  $E_g$  value obtained for CeTi and pure Ti are 3.15 eV and 3.29 eV, respectively. These  $E_g$  values could be important for application of the synthesized sample in photo-assisted studies.

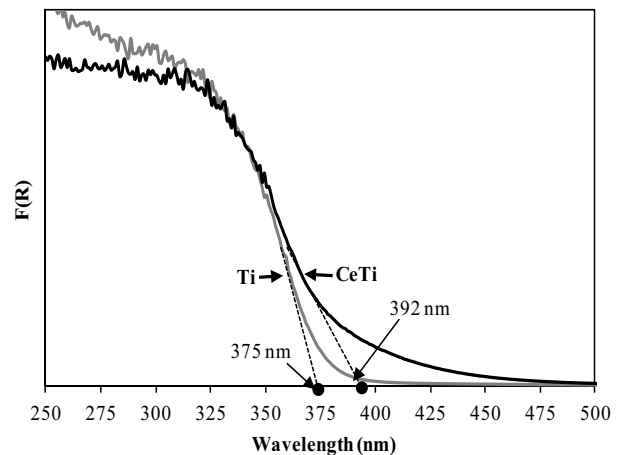
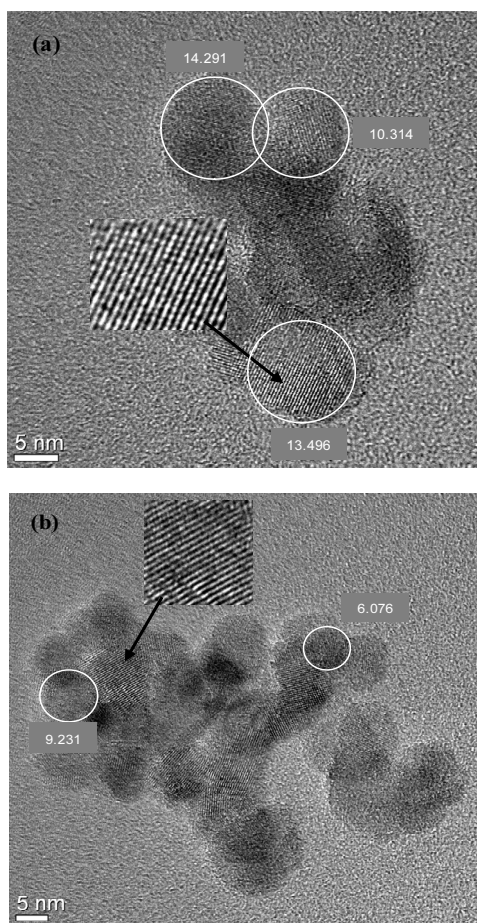


Fig. 4. A plot between Kubelka–Munk function and absorption wavelength of the synthesized composite nanocrystal

Typical cluster morphology of high resolution TEM images of the pure Ti and CeTi are shown in Fig. 5, a and 5, b, respectively. In the bright field image, all the synthesized sample seem to consist of many round shaped particles with moderated aggregation. The average particle size of pure Ti sample (Fig. 5, a) was estimated in the range of 10 nm–15 nm. While CeTi particle size (Fig. 5, b) was found in the range of 6 nm–10 nm. The lattice fringes (inset of Fig. 5, a–b) indicate that the composite samples are in good crystalline nature. Generally, the results from the TEM study are in accordance with the XRD data.

### 3.2. Dye adsorption performance

The performance of the synthesized samples were tested for its ability to adsorb a synthetic dye compound with the CR as the model pollutant. Fig. 6 shows the time-dependent CR adsorption by Ti and CeTi at room temperature. As can be seen in Fig. 6, both pure Ti and CeTi samples showed strong adsorptive capacity for CR dye. The removal efficiency of both samples show similar trend where adsorption rate increase rapidly at first 5 min, and then keep steady as time increase. The equilibrium



**Fig. 5.** HR-TEM images of Ti (a) and CeTi (b) synthesized composite nanocrystal

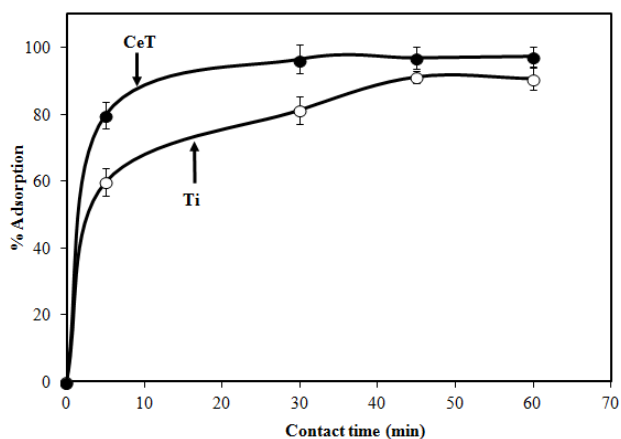


**Fig. 6.** Effect of contact time on CR adsorption over synthesized composite nanocrystals (Error bars represent standard deviation of the three experiment replications, corresponding to a value in the range of  $\pm(1.84-4.38)\%$ )

time of pure Ti and CeTi were found to be 45 min and 30 min, respectively. The ability of CeTi to adsorb the CR dye was higher than the pure Ti, which can obviously be observed from the curve. Smaller particle size of CeTi than that of pure Ti may play important role in the adsorption process of CR dye. The smaller in particle size is associated with a higher surface area. In adsorption study, large surface area that means small particles size is favoured because more active sites are available for adsorbate molecules that can attach to the surface of adsorbent. However, more

detailed study to understand the adsorption performance of the synthesized nanocrystals is essential.

## 4. CONCLUSIONS

High crystallinity property of pure anatase Ti and CeTi composite nanocrystals were synthesized by coprecipitation method. The characterization of both samples were presence in the form of pure anatase phase with nano scale in the particle size. The effect of Ce in changing the properties of Ti was evidenced by comparing the data from XRD, FT-IR, and TEM studies. Also, the optical band gap energy of CeTi (3.15 eV) was lower than pure Ti (3.29 eV), indicating that the synthesized sample could become a candidate catalyst for application in photo-assisted studies. The adsorption performance studies showed that the ability of CeTi to adsorb the CR dye was higher than pure Ti. However, more detailed study to understand the adsorption performance of the synthesized nanocrystals is essential. In addition, comprehensive study on the synergies effect between adsorption ability and optical properties of the synthesized sample, so called photocatalytic study, is also interesting to be done.

## Acknowledgments

The authors grateful to Hendris Hendarsyah Kurniawan, Division of Environmental Technology, RCC-LIPI for providing the commercial CR dye.

## REFERENCES

1. **Knizikevicius, R.** Simulation of Reactive Sputter Deposition of TiO<sub>2</sub> Films *Materials Science (Medziagotyra)* 16 2010: pp. 202–204.
2. **Cyviene, J., Milcius, D., Laukaitis, G.** Porosity Evaluation of TiO<sub>2</sub> Thin Films Deposited using Pulsed DC-Magnetron Sputtering *Materials Science (Medziagotyra)* 15 2009: pp. 103–107.
3. **Mirjalili, B. B. F., Akbari, A.** Nano-TiO<sub>2</sub>: An Eco-friendly Alternative for the Synthesis of Quinoxalines *Chinese Chemical Letters* 22 2011: pp. 753–756. <http://dx.doi.org/10.1016/j.ccllet.2010.12.016>
4. **Wu, M. C., Sapi, A., Avila, A., Szabo, M., Hiltunen, J., Huuhtanen, M.** Enhanced Photocatalytic Activity of TiO<sub>2</sub> Nanofibers and Their Flexible Composite Films: Decomposition of Organic Dyes and Efficient H<sub>2</sub> Generation from Ethanol–Water Mixtures *Nano Research* 44 2011: pp. 360–369.
5. **Reddy, B., Reddy, G., Rao, K., Ganesh, I., Ferreira, J.** Characterization and Photocatalytic Activity of TiO<sub>2</sub>-M<sub>x</sub>O<sub>y</sub> (M<sub>x</sub>O<sub>y</sub> = SiO<sub>2</sub>, Al<sub>2</sub>O<sub>3</sub>, and ZrO<sub>2</sub>) Mixed Oxides Synthesized by Microwave-Induced Solution Combustion Technique *Journal of Materials Science* 44 2009: pp 4874–4882. <http://dx.doi.org/10.1007/s10853-009-3743-x>
6. **Yang, S., Zhua, W., Wang, J., Chen, Z.** Catalytic Wet Air Oxidation of Phenol over CeO<sub>2</sub>-TiO<sub>2</sub> Catalyst in the Batch Reactor and the Packed-Bed Reactor *Journal of Hazardous Materials* 153 2008: pp. 1248–1253. <http://dx.doi.org/10.1016/j.jhazmat.2007.09.084>
7. **Bandara, J., Udawatta, C. P. K., Rajapakse, C. S. K.** Highly Stable CuO Incorporated TiO<sub>2</sub> Catalyst for Photocatalytic Hydrogen Production from H<sub>2</sub>O *Photochemical & Photobiological Sciences* 4 2005: pp. 857–861.

8. **Zhang, X., Lei, L.** Preparation of Photocatalytic Fe<sub>2</sub>O<sub>3</sub>-TiO<sub>2</sub> Coatings in One Step by Metal Organic Chemical Vapor Deposition *Applied Surface Science* 254 2008: pp. 2406–2412.  
<http://dx.doi.org/10.1016/j.apsusc.2007.09.067>
9. **Shi, L., Li, C., Gu, H., Fang, D.** Morphology and Properties of Ultrafine SnO<sub>2</sub>-TiO<sub>2</sub> Coupled Semiconductor Particles *Materials Chemistry and Physics* 62 2000: pp. 62–67.  
[http://dx.doi.org/10.1016/S0254-0584\(99\)00171-6](http://dx.doi.org/10.1016/S0254-0584(99)00171-6)
10. **Mishra, T., Hait, J., Aman, N., Gunjan, M., Mahato, B., Jana, R. K.** Surfactant Mediated Synthesis of Spherical Binary Oxides Photocatalytic with Enhanced Activity in Visible Light *Journal of Colloid and Interface Science* 327 2008: pp. 377–383.  
<http://dx.doi.org/10.1016/j.jcis.2008.08.040>
11. **He, J., Cai, Q. Z., Luo, Q., Zhang, D. Q., Tang, T. T., Jiang, Y. F.** Photocatalytic Removal of Methyl Orange in An Aqueous Solution by a WO<sub>3</sub>/TiO<sub>2</sub> Composite Film *Korean Journal of Chemical Engineering* 27 2010: pp. 435–438
12. **Zhao, Y., Li, C., Liu, X., Gu, F., Du, H. L., Shi, L.** Zn-doped TiO<sub>2</sub> Nanoparticles with High Photocatalytic Activity Synthesized by Hydrogen-Oxygen Diffusion Flame *Applied Catalysis B: Environmental* 79 2008: pp. 208–215.  
<http://dx.doi.org/10.1016/j.apcatb.2007.09.044>
13. **Xin, B., Wang, P., Ding, D., Liu, J., Ren, Z., Fu, H.** Effect of Surface Species on Cu-TiO<sub>2</sub> Photocatalytic Activity *Applied Surface Science* 254 2008: pp. 2569–2574.  
<http://dx.doi.org/10.1016/j.apsusc.2007.09.002>
14. **Zou, J. J., Zhu, B., Wang, L., Zhang, X., Mi, Z.** Zn- and La-Modified TiO<sub>2</sub> Photocatalysts for the Isomerization of Norbornadiene to Quadricyclane *Journal of Molecular Catalysis A: Chemical* 286 2008: pp. 63–69.  
<http://dx.doi.org/10.1016/j.molcata.2008.01.045>
15. **Chen, C., Wang, Z., Ruan, S., Zou, B., Zhao, M., Wu, F.** Photocatalytic Degradation of C.I. Acid Orange 52 in the Presence of Zn-doped TiO<sub>2</sub> Prepared by A Stearic Acid Gel Method *Dyes and Pigments* 77 2008: pp. 204–209.  
<http://dx.doi.org/10.1016/j.dyepig.2007.05.003>
16. **Kozlova, E. A., Korobkina, T. P., Vorontsov, A. V., Parmon, V. N.** Enhancement of the O<sub>2</sub> or H<sub>2</sub> Photoproduction Rate in a Ce<sup>3+</sup>/Ce<sup>4+</sup>-TiO<sub>2</sub> System by the TiO<sub>2</sub> Surface and Structure Modification *Applied Catalysis A: General* 367 2009: pp. 130–137.  
<http://dx.doi.org/10.1016/j.apcata.2009.07.045>
17. **Watanabe, S., Ma, X., Song, C.** Selective Sulfur Removal from Liquid Hydrocarbon Over Regenerable CeO<sub>2</sub>-TiO<sub>2</sub> Adsorbent for Fuel Cell Application *American Chemical Society: Division of Fuel Chemistry* 49 2004: pp. 511–513.
18. **Kefi, B. B., Atracheb, L. L. E., Kochkar, H., Ghorbel, A.** TiO<sub>2</sub> Nanotubes as Solid-Phase Extraction Adsorbent for the Determination of Polycyclic Aromatic Hydrocarbons in Environmental Water Samples *Journal of Environmental Sciences* 23 2011: pp. 860–867.  
[http://dx.doi.org/10.1016/S1001-0742\(10\)60481-0](http://dx.doi.org/10.1016/S1001-0742(10)60481-0)
19. **Luo, Y., Li, D.** Experimental Study of Nanometer TiO<sub>2</sub> for Use as An Adsorbent for SO<sub>2</sub> Removal *Developments in Chemical Engineering and Mineral Processing* 10 2002: pp. 443–457.
20. **Deng, S., Lia, Z., Huang, J., Yua, G.** Preparation, Characterization and Application of a Ce-Ti Oxide Adsorbent for Enhanced Removal of Arsenate from Water *Journal of Hazardous Materials* 179 2010: pp. 1014–1021.  
<http://dx.doi.org/10.1016/j.jhazmat.2010.03.106>
21. **Kim, S. J., Lee, E. G., Park, S. D., Jeon, C. J., Cho, Y. H., Rhee, C. K.** Photocatalytic Effects of Rutile Phase TiO<sub>2</sub> Ultrafine Powder with High Specific Surface Area Obtained by A Homogeneous Precipitation Process at Low Temperatures *Journal of Sol-Gel Science and Technology* 22 2001: pp. 63–74.
22. **Zuas, O., Budiman, H., Hamim, N.** Anatase TiO<sub>2</sub> and Mixed M-Anatase TiO<sub>2</sub> (M = CeO<sub>2</sub> or ZrO<sub>2</sub>) Nano Powder: Synthesis and Characterization *International Journal of Nano Dimension* 4 2013: (in press)
23. **Masuda, Y., Kato, K.** Synthesis and Phase Transformation of TiO<sub>2</sub> Nano-Crystal in Aqueous Solutions *Journal of the Ceramic Society of Japan* 117 2009: pp. 373–376.
24. **Sasirekha, N., Basha, S. J. S., Shanthi, K.** Photocatalytic Performance of Ru Doped Anatase Mounted on Silica for Reduction of Carbon Dioxide *Applied Catalysis B: Environmental* 62 2006: pp. 169–180.  
<http://dx.doi.org/10.1016/j.apcatb.2005.07.009>
25. **Ge, L., Xu, M., Sun, M., Fang, H.** Low-Temperature Synthesis of Photocatalytic TiO<sub>2</sub> Thin Film from Aqueous Anatase Precursor Sols *Journal of Sol-Gel Science and Technology* 38 2006: pp. 47–53.
26. **Dhage, S. R., Gaikwad, S. P., Ravi, V.** Synthesis of Nanocrystalline TiO<sub>2</sub> by Tartarate Gel Method *Bulletin of Material Science* 27 2004: pp. 487–489.
27. **Mohammadi, M. R., Fray, D. J., Sadrnezhaad, S. K., Mohammadi, A.** A Simple Particulate Sol-Gel Route to Synthesize Nanostructural TiO<sub>2</sub>-Ta<sub>2</sub>O<sub>5</sub> Binary Oxides and Their Characteristics *Materials Science and Engineering B* 142 2007: pp. 16–27.  
<http://dx.doi.org/10.1016/j.mseb.2007.06.023>
28. **Zou, J., Gao, J., Xie, F.** An Amorphous TiO<sub>2</sub> Sol Sensitized with H<sub>2</sub>O<sub>2</sub> with the Enhancement of Photocatalytic Activity *Journal of Alloys and Compounds* 497 2010: pp. 420–427.  
<http://dx.doi.org/10.1016/j.jallcom.2010.03.093>
29. **Hernández, A., Maya, L., Sánchez-Mora, E., Sánchez, E. M.** Sol-Gel Synthesis, Characterization and Photocatalytic Activity of Mixed Oxide ZnO-Fe<sub>2</sub>O<sub>3</sub> *Journal of Sol-Gel Science and Technology* 42 2007: pp. 71–78.
30. **Nidhin, M., Indumathy, R., Sreeram, K. J., Nair, B. U.** Synthesis of Iron Oxide Nanoparticles of Narrow Size Distribution on Polysaccharide Templates *Bulletin of Material Science* 31 2008: pp. 93–96.
31. **Gao, S. A., Xian, A. P., Cao, L. H., Xie, R. C. Shangm, J. K.** Influence of Calcining Temperature on Photoresponse of TiO<sub>2</sub> Film under Nitrogen and Oxygen in Room Temperature *Sensors and Actuators B: Chemical* 134 2008: pp. 718–726.
32. **Chiang, K., Amal, R., Tran, T.** Photocatalytic Degradation of Cyanide using Titanium Dioxide Modified with Copper Oxide *Advances in Environmental Research* 6 2002: pp. 471–485.  
[http://dx.doi.org/10.1016/S1093-0191\(01\)00074-0](http://dx.doi.org/10.1016/S1093-0191(01)00074-0)